

RESEARCH ARTICLE

10.1029/2018JB015824

Special Section:

Gas Hydrate in Porous Media: Linking Laboratory and Field Scale Phenomena

Key Points:

- Unlike hydrate-bearing sands, the behavior of hydrate-bearing clays proved contractive upon shearing according to in situ data
- Hydromechanical properties of hydrate-bearing clays depend on hydrate content and superimposed influence of their distribution/morphology
- For gas hydrate contents higher than 20%, the hydraulic diffusivity increases with hydrate concentration

Correspondence to:

F. Taleb, farah.taleb@ifremer.fr

Citation:

Taleb, F., Garziglia, S., & Sultan, N. (2018). Hydromechanical properties of gas hydrate-bearing fine sediments from in situ testing. *Journal of Geophysical Research: Solid Earth*, 123, 9615–9634. <https://doi.org/10.1029/2018JB015824>

Received 23 MAR 2018

Accepted 6 NOV 2018

Accepted article online 10 NOV 2018

Published online 28 NOV 2018

©2018. The Authors.

This is an open access article under the terms of the Creative Commons Attribution-NonCommercial-NoDerivs License, which permits use and distribution in any medium, provided the original work is properly cited, the use is non-commercial and no modifications or adaptations are made.

Hydromechanical Properties of Gas Hydrate-Bearing Fine Sediments From In Situ Testing

F. Taleb¹ , S. Garziglia¹, and N. Sultan¹ 

¹Département REM, Unité des Géosciences Marines, IFREMER, Plouzané, France

Abstract The hydromechanical properties of gas hydrate-bearing sediment are key in assessing offshore geohazards and the resource potential of gas hydrates. For sandy materials, such properties were proved highly dependent on hydrate content (S_h) as well as on their distribution and morphology. Owing to difficulties in testing gas hydrate-bearing clayey sediments, the impact of hydrates on the behavior of such materials remains poorly understood. Hence, to provide insight into the characterization of clayey sediments containing hydrate, this study relies on a unique database of in situ acoustic, piezocone, and pore pressure dissipation measurements collected in a high gas flux system offshore Nigeria. Compressional wave velocity measurements were used as means of both detecting and quantifying gas hydrate in marine sediments. The analysis of piezocone data in normalized soil classification charts suggested that contrary to hydrate-bearing sands, the behavior of gas hydrate-bearing clays tends to be contractive. Correlations of acoustic and geotechnical data have shown that the stiffness and strength tend to increase with increasing S_h . However, several sediment intervals sharing the same S_h have revealed different features of mechanical behavior; suggesting that stiffness and strength of gas hydrate-bearing clays are influenced by the distribution/morphology of gas hydrate. Pore pressure dissipation data confirmed the contractive behavior of gas hydrate-bearing clays and showed that at low hydrate content, the hydraulic diffusivity (C_h) decreases when S_h increases. However, for S_h exceeding 20%, it was shown that an increase of C_h with S_h could be linked to the presence of fractures in the hydrate-sediment system.

1. Introduction

Over the last decades, increasing world's energy demand amidst of climate change concerns have encouraged the search for alternative and cleaner energy resources. Gas hydrate (GH) are considered as the largest untapped stock of natural gas in the world (Boswell & Collett, 2011) and are characterized by their widespread occurrence mainly in permafrost regions and continental margins (Kvenvolden, 1993). Due to the estimated staggering amounts of GH and their potential as a future energy resource but furthermore as a geotechnical hazard for various offshore operations and hydrocarbon recovery projects (Kayen & Lee, 1991) and their possible contribution to current and future climate change scenarios (Yun et al., 2007), GH have stimulated international academic and industrial interest.

The formation of GH within the sediment significantly alters the physical and mechanical properties of their host sediment. Such properties are also proved dependent on the hydrate content within the sediment as well as on their morphology/distribution (Dai et al., 2012). Thus, the quantification and characterization of GH within the marine environment have become significantly important in order to either contain their potential geotechnical threat or understand their effect on the hydromechanical properties of the host sediment under stability conditions (Ning et al., 2012).

GH can occur in a variety of sediments such as fine-grained clays and coarse-grained sands. Due to their high permeability and high GH content, coarse-grained sediments are often preferred for potential exploitation activities. However, fine-grained sediments contain over 90% of global GH accumulations (Boswell & Collett, 2006), yet not much research have been carried out concerning the hydromechanical behavior of such sediments.

The formation of GH within the sediment is mainly governed by the changing physical properties of the latter such as grain size, porosity, and permeability (Waite et al., 2009). This directly affects the morphology of the hydrate within the host sediment. Sands and coarse silts are characterized by disseminated pore-filling hydrate (Waite et al., 2009). The grain-displacing morphology is mostly observed in clay-rich sediments where GH form in fractures due to capillary tension forces (Jang & Santamarina, 2016). In this case, they force the

clay aggregates to move apart and hence introduce veins or cracks within the sediment. However, Ghosh et al. (2010) suggested that in clayey sediments, GH could be present as pore-filling, grain-displacing, or a combination of both morphologies. This imposes a complexity when it comes to GH quantification in such sediments, since it requires knowledge of the orientation of the GH-bearing discontinuities.

The metastable nature of GH and the challenges they present in terms of identifying their presence via the recovery of natural samples have largely increased the reliance on pressure coring to prevent sediment disturbance (Santamarina et al., 2012). However, as presented by Sultan et al. (2007, 2010, 2014) in situ testing may be a promising alternative to costly pressure coring and testing operations. As reported in much literature, in situ testing is an efficient and cost-effective technique of collecting large amounts of data mainly in materials that are difficult to sample (Lunne et al., 1997; Robertson, 2009). This is particularly efficient in the case of GH-bearing fine-grained sediments, which remain challenging to preserve or synthesize prior to laboratory testing. Hence, to provide insight into the characterization of these geomaterials, this study relies on in situ acoustic, piezocone, and pore pressure dissipation measurements in the Gulf of Guinea.

Numerous oceanographic campaigns have been carried out along the West African margin due to the ongoing development of oil and gas projects. The Gulf of Guinea is one area where the presence of dense accumulations of shallow GH have been reported by several authors (Cunningham & Lindholm, 2000; Hovland et al., 1997; Sultan et al., 2010; Wei et al., 2015). Visual observations within the study area have revealed the presence of different GH morphologies varying from groups of thin veins to massive nodules in clay sediments (Sultan et al., 2007, 2010). In certain cases, solid GH and free gas were observed to coexist due to the presence of free gas voids within hydrate nodules; hence, resulting in a material with a spongy texture (Sultan et al., 2014).

The present work aims to understand the effect of the concentration and distribution/morphology of GH on the hydromechanical properties of their host clayey sediment. This relies on the quantification and characterization of GH using different in situ acoustic and geotechnical methods. The investigation was carried out by correlating these parameters and comparing sites without GH to GH-bearing sites. Different soil classification charts were used to illustrate the behavior of hydrate-bearing clays. Finally, different hydromechanical parameters of GHs bearing fine-grained sediments were derived using empirical relations.

2. Study Area

The study area is located in the deep water Niger Delta at a water depth ranging from 1,100 to 1,250 m. Numerous studies (Sultan et al., 2010, 2014) have shown that this area is characterized by several quasi-circular pockmarks (Figure 1) that are ten to a few hundred meters wide. The evolution and morphologies of these pockmarks have been directly linked to different habits of formation, nucleation, and dissolution of GH (Sultan et al., 2014). Wei et al. (2015) have investigated the distribution of GH in the sediment of the study area by applying infrared thermal imaging and pore water chloride analyses on MeBo cores, which allowed defining hydrate occurrence zones. These zones were shown to accommodate shallow GH accumulations (Sultan et al., 2007) as well as the coexistence of free gas and solid GHs. Based on the latter findings and on seismic data showing evidence of faulting (Sultan et al., 2016), the investigated area has been identified as a high gas flux system.

3. Tools and Methods

The data used in this paper were acquired during the Guineco-MeBo (2011) and ERIG3D (2008) oceanographic campaigns on the French R/V *Pourquoi pas?*. Both campaigns aimed to determine the distribution of GH from geophysical, geotechnical, and geochemical data. Different laboratory and in situ measurements were carried out to assess the physicochemical properties of the sediment at a number of sites outside and within pockmarks as shown in Figure 1 and Table 1.

3.1. In Situ Measurements and Coring

3.1.1. Piezocone (Penfeld)

In situ acoustic and geotechnical measurements were carried out using the Penfeld seabed rig developed by Ifremer. It is provided with a rod that can push two types of probes down to 30 m below seabed with a thrust of 40 kN at a standard rate of 2 cm/s (Sultan et al., 2007).

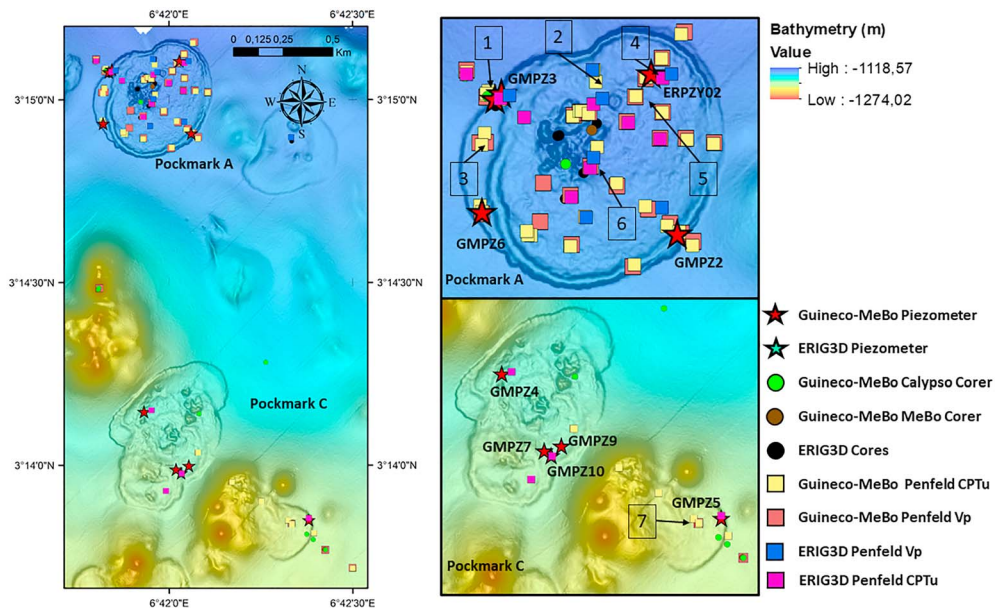


Figure 1. Bathymetry of the study area showing the investigated sites: 1: GMPFV02S02, GMPFM06S01, GMPZ3, GMMB01, and GMCS05; 2: ERVP03S01 and GMPFM12S03; 3: GMPFV02S03 and GMPFM01S03; 4: GMPFV03S03, ERCPT02S08, ERPZY02 and GMMB12; 5: GMPFV03S04 and GMPFM04S04; 6: GMPFV07S05, ERCPT02S05, and GMMB06; and 7: GMPFV10S04, GMPFM05S03, and GMMB05.

The piezocone probe can be used to carry out Cone Penetration Testing with pore pressure measurement (CPTu); thus, providing continuous vertical readings of cone tip resistance (q_t), sleeve friction (f_s), and penetration pore pressure (Δu_2). The latter is measured with a differential pore pressure sensor located immediately behind the cone (u_2 position). The piezocone is equipped with pressure-compensated sensors to provide accurate measurements irrespective of the water depth.

The ultrasonic fork can alternatively be used to measure every 2 cm the velocity of compressional waves (Vp) up to 2,200 m/s. Acoustic measurements are carried out by producing a 1-MHz compressional wave from one branch of the fork and recording its travel time to the opposite branch located 7 cm apart. The amplitude ratio between the input and received signals provides attenuation. As an additional parameter recorded during acoustic measurements, the so-called *applied load* corresponds to the force required to push the ultrasonic fork in the sediment.

In this paper, seven Penfeld Vp (1: GMPFV02S02, 2: ERVP03S01, 3: GMPFV02S03, 4: GMPFV03S03, 5: GMPFV03S04, 6: GMPFV07S05, and 7: GMPFV10S04) and seven Penfeld CPTu (1: GMPFM06S01, 2: GMPFM12S03, 3: GMPFM01S03, 4: ERCPT02S08, 5: GMPFM04S04, 6: ERCPT02S05, and 7: GMPFM05S03) were investigated, as seen in Figure 1 and Table 1.

Table 1
Investigated Sites Within the Study Area

Investigated site	Depth (m)	Length (m)	Nearby CPTu	Nearby piezocone	Nearby Calypso or MeBo core	Site
GMPFV02S02	1,140	30	GMPFM06S01	GMPZ3	GMCS05	1
ERVP03S01	1,140	30	GMPFM12S03	—	—	2
GMPFV02S03	1,144	30	GMPFM01S03	—	—	3
GMPFV03S03	1,142	10.3	ERCPT02S08	ERPZY02	GMMB12	4
GMPFV03S04	1,140	5.7	GMPFM04S04	—	—	5
GMPFV07S05	1,146	8.5	ERCPT02S05	—	GMMB06	6
GMPFV10S04	1,195	26	GMPFM05S03	—	GMMB05	7

Note. Site 1 cluster was used to characterize sediment from the reference site without gas hydrate while sites 2, 3, 4, 5, 6 and 7 clusters represent areas where the presence of gas hydrate was suspected or proved.

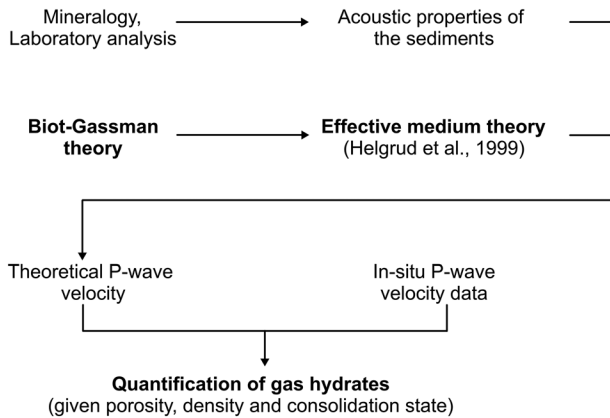


Figure 2. Adopted method to apply the effective medium theory (Helgerud et al., 1999).

3.1.2. Piezometer

The Ifremer piezometer is a free-fall device that allows pore pressure measurements. It is equipped with a 60-mm-diameter sediment-piercing lance whose length can be adapted to the type and the stiffness of the penetrated sediment. For example, a 12-m-length lance is used for soft sediments. Pore pressures are measured at up to 10 ports with a minimum spacing of 70 cm using differential pressure transducers. They measure pressure relative to hydrostatic pressure with an accuracy of 0.4 kPa. The lance is also equipped with temperature sensors having an accuracy of 0.05 °C.

The piezometer can be used in two modes: long- and short-term measurements. In the former, equilibrium pore pressure can be reached after several days; whereas in the latter the equilibrium pore pressure is evaluated following the technique proposed by Sultan and Lafuerza (2013).

In this paper 10 piezometer sites will be investigated (GMPZ2, 3, 4, 5, 6, 7, and 10 and ERPZY02), with only two next to a Penfeld V_p site (1: GMPZ3 and 4: ERPZY02).

3.1.3. Coring and Drilling

Core sediments used in this paper are obtained from a Calypso coring system. It is equipped with a Kullenberg type piston that minimizes the variations of the internal pressure during the coring process. Hence, the sediment is less disturbed when recovered to the surface. The Calypso Corer allows the recovery of up to 35 m of marine sediment.

The seafloor drill rig MeBo (Freudenthal & Wefer, 2007; Freudenthal & Wefer, 2013) was also used to recover longer sedimentary cores.

In this work, one Calypso core (1: GMCS05) and four MeBo cores (1: GMMB01, 4: GMMB12, 6: GMMB06, and 7: GMMB05) have allowed the investigation of the study area (Figure 1 and Table 1).

3.2. Laboratory Testing

3.2.1. MSCL and XRD

The Multi-Sensor Core Logger (MSCL) from Geotech was used onboard in order to measure the P wave velocity, the Gamma density, and the magnetic susceptibility on 1-m-long whole core sections. This was done at 1-cm step for all cores without hydrate and at 2-cm step for cores containing hydrate. In this work, the density profile from Calypso core GMCS05 (site 1 in Figure 1) was taken as representative of the study area.

The X-ray diffraction (XRD) method was used to characterize the mineralogical composition of sediment sampled with a 10-cm spacing on core GMCS05. By correlating X-ray diffraction results with those obtained with an Avaatech X-ray fluorescence core scanner, the clay, calcite, and quartz fractions in sediment from core GMCS05 were determined with a finer spacing of 2 cm. (Figure 2).

3.3. GH Quantification

3.3.1. From Pore Water Chloride Analysis

The formation of GH is known to exclude ions dissolved in pore water from the clathrate cage, hence, increasing the salinity of the surrounding pore water (Paul & Ussler, 2001). Therefore, the dissociation of GH upon core recovery releases fresh water, causing negative anomalies on pore water chloride profiles (Wei et al., 2015).

As reported by Wei et al., (2015), pore water was extracted using Rhizon samplers on 12 MeBo cores collected in the study area. Chloride concentrations were subsequently determined using ion chromatography (Wei et al., 2015). This led Wei et al., (2015) to determine a baseline pore water chlorinity in the absence of GH of 550 mM. This was done by measuring chloride concentrations in bottom waters and in reference sediments.

This value served as an input parameter in the estimation of the GH content S_h from chloride anomalies following the method presented by Malinverno et al. (2008):

Table 2
Elastic and Density Properties of Selected Sediment Components (After Helgerud et al., 1999)

Constituent m	K (GPa)	G (GPa)	ρ (g/cm ³)
Clay	20.9	6.85	2.58
Calcite	76.8	32	2.71
Quartz	36.6	45	2.65
Gas hydrate	7.9	3.3	0.90
Water	2.4–2.6	0	1.032
Methane gas	0.10–0.12	0	0.23

Note. K is the bulk modulus, G the shear modulus, and ρ the density.

$$S_h = \frac{\beta(C_{cb} - C_c)}{C_c + \beta(C_{cb} - C_c)} \quad (1)$$

where β is a coefficient that accounts for the density change from GH to water and equals 1.257, C_{cb} is the baseline pore water chlorinity prior to dissociation, and C_c is the chlorinity measured in the core after dissociation.

3.3.2. From In Situ Vp Measurements and Rock Physics Characterization

The effective medium model developed by Helgerud et al. (1999) was used to estimate GH content within the marine sediment from in situ Vp measurements. The principle of this model is to relate the stiffness of the dry

frame to porosity, mineralogy, and effective stress. As key input parameters to the model, the sediment mineralogy, porosity, and its evolution with effective stress were determined from analyses of core GMCS05 taken as representative of the study area. The elastic properties and densities used in the calculation were similar to those used by Helgerud et al. (1999) as shown in Table 2.

Differences between calculated and measured *P* wave velocities (Figure 2) were used to obtain an upper- and lower-bound estimate of GH content within the sediment by assuming that: (a) hydrate alters only the pore fluid elastic properties (S_{hmax}); (b) hydrate contributes stiffness to the sediment by becoming part of the load-bearing framework (S_{hmin}).

It is noteworthy that considering one case or the other has implications on the derivation of the lithostatic stress as explained by Helgerud et al. (1999). However, when calculating the effective stress as the difference between the lithostatic stress and the pore fluid pressure, hydrostatic conditions were always assumed for the latter.

3.4. Derivation of Geotechnical Properties From Piezocone Results

Piezocone readings including q_t , f_s , and Δu_2 were, first, used to classify sediments based on their behavior characteristics and, second, to derive their geotechnical properties. The classification process relied on the method suggested by Robertson (2016) using the following equations:

The normalized friction ratio

$$F_r = 100 \times \frac{f_s}{q_t - \sigma_{v0}} \quad [\%] \quad (2)$$

The normalized pore pressure

$$U_2 = \frac{\Delta u_2}{\sigma'_{v0}} \quad [-] \quad (3)$$

A revised value of normalized cone resistance

$$Q_{tn} = \left(\frac{q_t - \sigma_{v0}}{p_a} \right) \left(\frac{p_a}{\sigma'_{v0}} \right)^n \quad [-] \quad (4)$$

Where p_a is the atmospheric reference pressure (i.e., 100 kPa) and n a stress exponent defined as

$$n = 0.381(l_c) + 0.05 \left(\frac{\sigma'_{v0}}{p_a} \right) - 0.15 \quad (5)$$

Where l_c is a soil behavior type index defined as

$$l_c = \left[\left(3.47 - \log \left[\frac{q_t - \sigma_{v0}}{\sigma'_{v0}} \right] \right) 2 + (\log F_r + 1.22) 2 \right]^{0.5} \quad (6)$$

For sediments without GH, the values of total and vertical effective stresses (σ_{v0} and σ'_{v0} , respectively) were

calculated from the unit weight profile obtained on core GMCS05. For GH-bearing sediment, the values were obtained from back calculations of GH content using the effective medium model developed by Helgerud et al., (1999; see section 3.3.2).

The geotechnical properties were empirically derived from piezocone results following the unified interpretation approach presented by Robertson (2009). Since the reliability and applicability of empirical correlations vary according to precedent and local experience, the properties derived from piezocone sounding in GH-bearing sediments must be treated with caution due to the lack of statistical study on this soil type.

Compression indices were estimated from piezocone results using the following equation:

$$\lambda = \frac{[(1 + e_0)\sigma'_{v0}]}{[\alpha_M(q_t - \sigma_{v0})]} \quad (7)$$

Where α_M is the constrained modulus cone factor. Based on correlations between piezocone data and results of oedometer tests reported by Sultan et al. (2007), a site-specific value of $\alpha_M = 1$ and a value of void ratio, $e_0 = 6.15$ (at $\sigma'_{v0} = 1$ kPa) were used to calculate compression indices for both hydrate-free and hydrate-bearing sediments.

Values of shear modulus at small strain (G_0) were estimated using

$$G_0 = 0.0188 \left[10^{(0.55I_c + 1.68)} (q_t - \sigma_{v0}) \right] \quad (8)$$

where I_c is the soil behavior type index previously defined (equation (8)). Following Krage et al. (2014) values of G_0 were converted into values of shear modulus at 50% mobilized strength (G_{50}) by assuming that $(G_{50}/G_0) = 0.26$ for both hydrate-free and hydrate-bearing sediments.

Values of peak undrained shear strength (Su) were derived from:

$$Su = \frac{(q_t - \sigma_{v0})}{N_{kt}} \quad (9)$$

where N_{kt} is a cone factor typically varying from 10 to 20. Following the works of Low et al. (2010) on soft clays, a N_{kt} value of 13.6 was used to calculate Su in hydrate-free sediments. A lower-bound estimate of the Su of GH-bearing sediments was calculated using a similar N_{kt} . Calculations were additionally performed using a N_{kt} value of 10 to provide an upper bound estimate.

Based on the assumption that values of sleeve friction (f_s) correspond to the remolded shear strength of the sediment, values of sensitivity were estimated using

$$St = \frac{Su}{f_s} \quad (10)$$

3.5. Derivation of Hydraulic Properties From Piezometer Results

The Ifremer piezometer was used to carry out pore pressure measurements at several selected locations and depths where the presence of GH was suspected and/or proved (GMPZ2, 4, 6, 7, and 10 and ERPZY02) as well as at two reference sites (GMPZ3 and 5). The measured pore water pressure (u) corresponds to an excess pore pressure (Δu) generated by the rod insertion and an in situ equilibrium pore pressure (u_{eq}), which is assumed constant during the dissipation of the measured maximum excess pore pressure ($u = \Delta u + u_{eq}$). The time for 50% dissipation of the measured maximum excess pore pressure (t_{50}) was determined using a graphical method in which u_{eq} was either reached from the dissipation test or calculated using the Sultan and Lafuerza (2013) numerical algorithm and after determining Δu_{100} , Δu_{0} , and Δu_{50} (see ASTM Standard D2435, 1996). It was then possible to derive the hydraulic diffusivity C_h (or the horizontal coefficient of consolidation) of the medium normalized by the square root of the rigidity index (I_r) using the following equation (Teh & Houlsby, 1991):

$$\frac{C_h}{\sqrt{I_r}} = \frac{C_p r^2}{t_{50}} \quad (11)$$

Where C_p is a factor related to the location of the sensor and r is the radius of the rod.

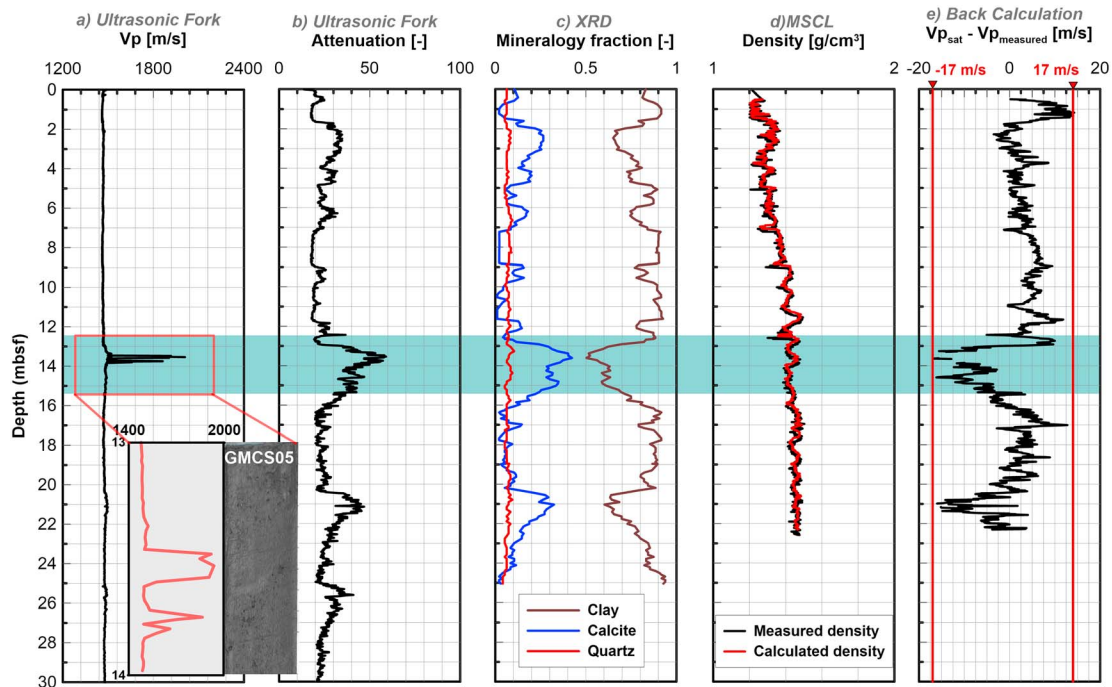


Figure 3. (a) *P* wave velocity and (b) signal attenuation for site GMPFV02S02, (c) mineral fraction and (d) vertical effective stress derived from Multi-Sensor Core Logger (MSCL) density data (core GMCS05) and model calculation (e) difference between calculated velocity and measured velocity. XRD = X-ray diffraction.

4. Results

4.1. Characterization of Sediment Without GH—Reference Site

Sites GMPFV02S02 and GMPFM06S01 (site 1 in Figure 1) were considered as Penfeld *V_p* and CPTu reference sites, respectively, since they are located outside of the pockmarks. Reference sites are characterized by compressional wave velocities varying between 1,450 m/s and 1,510 m/s. However at site GMPFV02S02, velocity and attenuation peaks of 2,015 m/s and 59, respectively, can be identified at 13.6 mbsf (Figures 3a and 3b). Additionally, while the quartz fraction profile is nearly constant along the core, the calcite and clay fractions vary from 0.5 to 0.9 and from 0.01 to 0.42, respectively (Figure 3c). It is noteworthy that there is great resemblance between the calcite, *V_p*, and signal attenuation profiles. Therefore, *V_p* peaks were linked to the presence of calcium carbonate (mainly foraminifera) within the sediment. This is further confirmed by visual observations of core GMCS05, which do not reveal any fractures or cracks as would be expected if GH were present at this site. The calculated vertical effective stress (σ'_{v0}) profile (Figure 3d) was determined with the model presented in section 3.3.2 assuming hydrostatic pressure and based on laboratory predefined compressibility and void ratio data. It can be observed that the measured σ'_{v0} and the calculated σ'_{v0} profiles yield almost the same results, confirming the reliability of the used model. Figure 3e shows that the difference between the velocity calculated by the model and the measured velocity tend to oscillate in the range ± 17 m/s. This served to set the detection threshold of GH in sediments. That is to say that, in this study, estimates of GH contents are only provided when the difference between the calculated *V_p* and measured *V_p* is greater than 17 m/s.

As shown in Figure 4, piezocone data for reference site GMPFM06S01 (site 1 in Figure 1) are characterized by a linear increase with depth of the corrected cone tip resistance (q_t), sleeve friction (f_s), and pore water pressure (Δu_2) up to 1,000, 12, and 320 kPa, respectively, at 30 mbsf.

By adopting the *P* wave velocity intercomparison method and considering sites GMPFV02S02 and GMPFM06S01 as a reference, the distinct features between GH-bearing sediments and sediments without hydrate were identified and discussed.

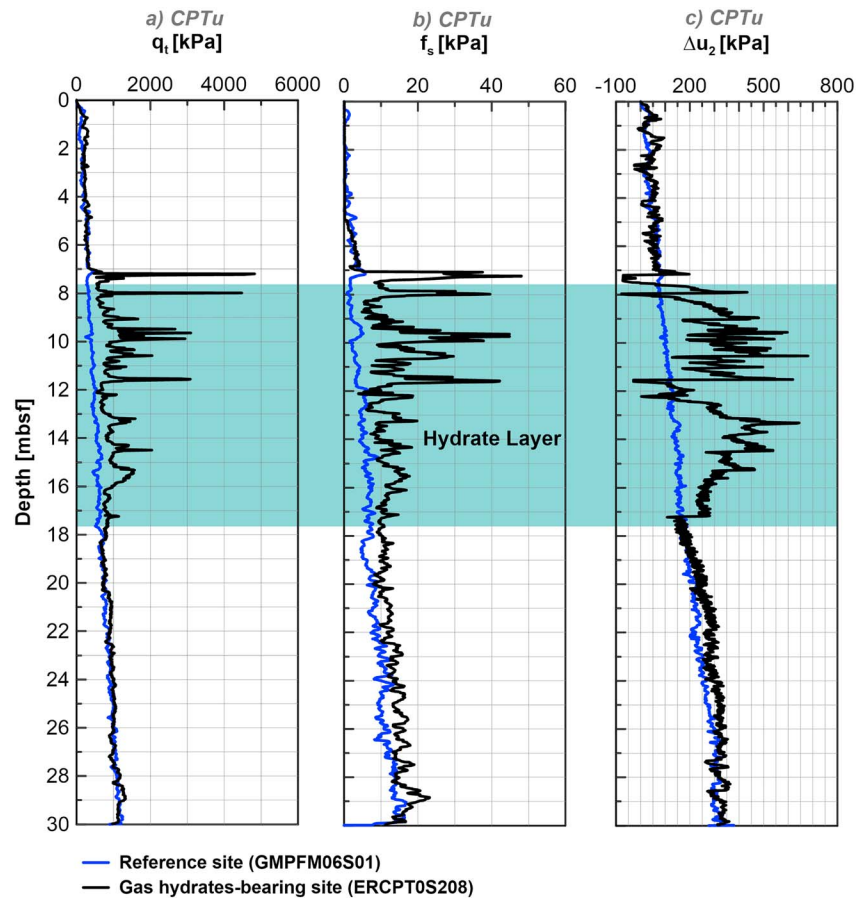


Figure 4. GH-bearing site ERCPT02S08 (site 4 in Figure 1): (a) Corrected cone tip resistance, (b) sleeve friction, and (c) pore water pressure. The light blue rectangle shows the GH occurrence zone identified by Wei et al. (2015) from chloride anomalies and infrared images. Cone Penetration Testing with pore pressure measurement.

4.2. GH Characterization and Quantification

Figure 4 presents the corrected cone tip resistance (q_t), the sleeve friction (f_s), and the pore water pressure (Δu_2) from the Penfeld CPTu for site ERCPT02S08 (site 4 in Figure 1). At 7.23 mbsf q_t was found to be almost 10 times higher than that of the reference site GMPFM06S01 at the same depth. Wei et al. (2015) identified the top of the GH occurrence zone at almost the same depth (see light blue rectangle in Figure 4).

The simultaneous and strong increase in these parameters (q_t , f_s , and Δu_2) confirms the presence of GH within the marine sediment. Additionally the q_t profile suggests the presence of two distinct GH layers: (1) from 7 to 11.5 mbsf with q_t ranging between 3,153 and 4,913 kPa and (2) from 12.5 to 17.5 mbsf with q_t ranging between 1,062 and 2,004 kPa. It is also noteworthy that at depths 7.23 and 8 mbsf, high f_s and q_t values correlate with negative Δu_2 values.

GHs were quantified at all sites where V_p data were available and after definition of the mineralogy profile of the sediment in question. Hydrate quantification results obtained from the numerical model using the effective medium theory were compared with those obtained from chloride anomalies using equation (1).

Figure 5 presents the P wave velocity (V_p), the signal attenuation and the applied load profiles obtained from the Penfeld V_p , and the back calculation for GH content for the GMPFV03S03 (site 4 in Figure 1) and the corrected cone tip resistance (q_t) obtained from Penfeld CPTu for the ERCPT02S08 (site 4 on Figure 1). Strong and positive variations of these parameters along the depth confirm the presence of GH. However, negative anomalies in the V_p profile is an indicator for the presence of free gas within the sediment. Therefore, it is possible to define areas where free gas and solid GH layers form alternatively or even coexist. CPTu = Cone Penetration Testing with pore pressure measurement.

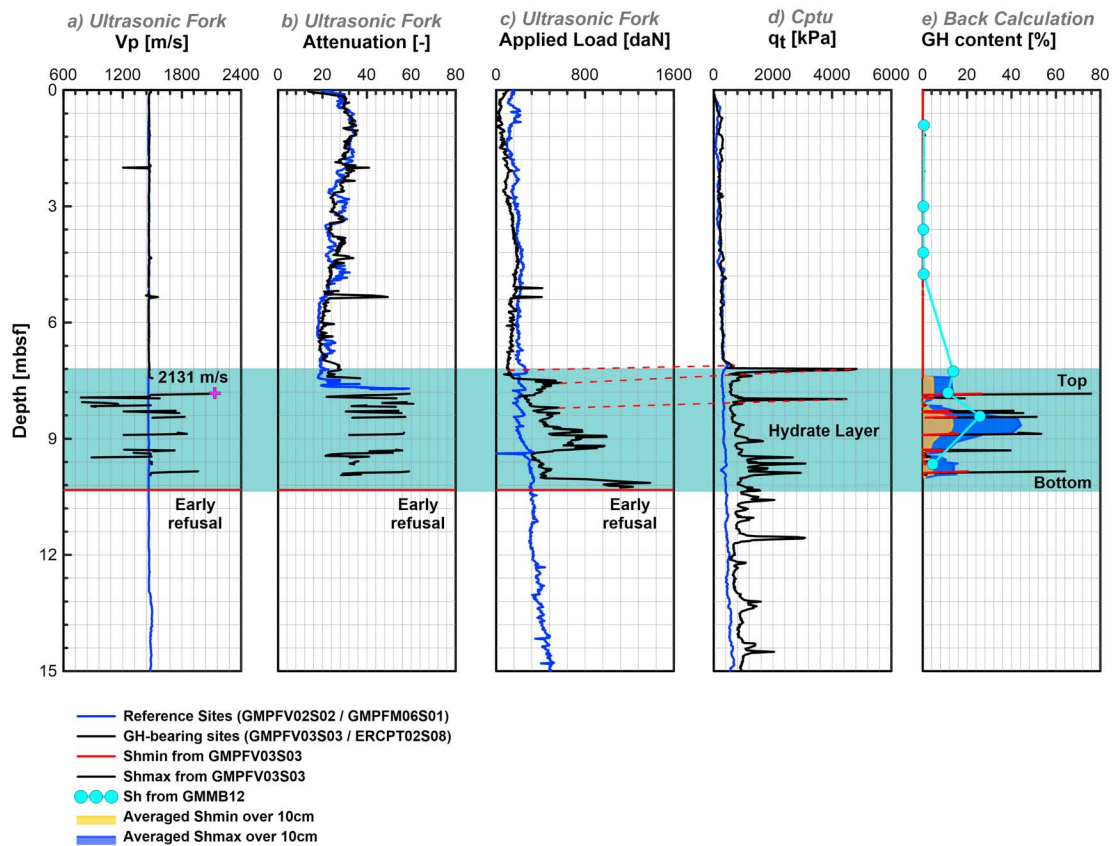


Figure 5. (a) P wave velocity, (b) signal attenuation, (c) applied load for GH-bearing site GMPFV03S03, (d) corrected cone tip resistance for GH-bearing site ERCPT02S08, and (e) back calculation of GH content.

While missing data is observed in the P wave velocity and attenuation profiles between 7.45 and 7.84 mbsf for the GMPFV03S03, the applied load profile suggests that GHs were reached at 7.45 mbsf (Figure 5). This was confirmed by the pore water chloride data that shows that the GH content reaches 14% at around 7.26 mbsf. This is followed by sudden increases of 2,131 m/s in V_p and 60 in the signal attenuation at 7.85 mbsf, which highlights the effect of the presence of GH within the marine sediment.

Using the effective medium theory, the GH content in the sediment was estimated and then averaged over 10 cm, allowing the comparison with estimates of GH content derived from chloride anomalies. Maximum GH content were estimated to occur at 7.85 mbsf: 27% for S_{hmin} , 76% for S_{hmax} , 6% for averaged S_{hmin} and 14.5% for averaged S_{hmax} . At this same depth, a GH content of 11.5% was estimated by the pore water chloride data, which almost equals the average value of averaged S_{hmin} and averaged S_{hmax} . Based on V_p anomalies, the top of the GH occurrence zone was assumed to start at 7.85 mbsf.

Quantification results derived from the effective medium theory and from the pore water chloride analysis for all investigated sites are presented in Figure 6. GH clearly exhibit a heterogeneous vertical distribution within the GH occurrence zones without showing any systematic pattern. By comparing both GH quantification methods for sites GMPFV03S03 (site 4 in Figure 1) and GMPFV10S04 (site 7 in Figure 1), it can be observed that averaged S_{hmax} and S_{hmin} values oscillate around values of S_h derived from the chlorinity data. On the other hand, for site GMPFV07S05 S_{hmax} values are closer to those derived from chlorinity data compared to S_{hmin} values. By contrast, nonaveraged values of S_{hmax} are much higher than those estimated from chlorinity data. Additionally, studies performed by Ghosh et al. (2010), showed that for GH-bearing clayey sediments S_{hmin} yields estimates closer to that obtained from the pressure core depressurization method compared to S_{hmax} . Hence, in the next chapters only S_{hmin} (called in the following s_h) values will be considered and discussed.

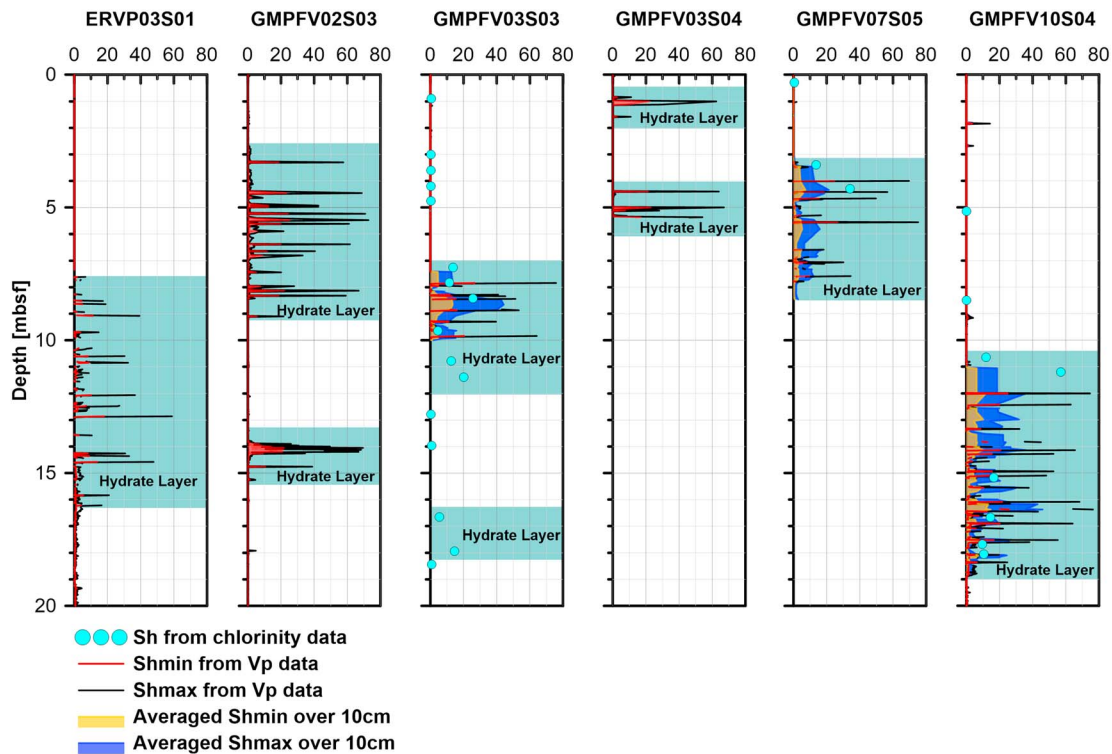


Figure 6. Estimates of gas hydrate content for all the six investigated sites: ERVP03S01 (site 2 in Figure 1), GMPFV02S03 (site 3 in Figure 1), GMPFV03S03 (site 4 in Figure 1), GMPFV03S04 (site 4 in Figure 1), GMPFV07S05 (site 6 in Figure 1), and GMPFV10S04 (site 7 in Figure 1).

4.3. Soil Behavior Classification Charts Using CPTu and Vp Data

To further highlight features of GH-bearing sediments, normalized CPTu data were plotted in Robertson (2016) updated classification charts. Figure 7 shows the data from GH-bearing sites (GMPFM12S03, GPFM04S04, GMPFM01S03, GMPFM05S03, ERCPT02S05, and ERCPT02S08) plotted as symbols whose shape represent GH content (S_h %) within the sediment. The diagrams charts also show the piezocone data where the GH content could not have been estimated. This is mainly due to missing Vp data (values higher than 2,200 m/s), which is a key parameter in the effective medium model. Correlations between in situ acoustic and geotechnical measurements were necessary in order to highlight the mechanical behavior of GH-bearing clayey sediment. This step was achieved by first identifying peaks and common patterns on the applied load and q_t profiles as it was thought to have the most physical meaning. As illustrated in Figure 5, correlations were made by relating depths of significant peaks in both profiles. This method was adopted for all other investigated sites. Due to difficulties in constantly correlating peaks, only 25 data points were considered in this work as unambiguous.

Based on the $Q_{tn} - U_2$ chart, sediment from reference sites exhibits U_2 values varying between 3 and 5.5 and Q_{tn} values not exceeding 16. Sediment containing GH is characterized by large Q_{tn} values up to 84 and correlating with U_2 values varying between 6 and 25. Most of the data from these sites plot in the contractive zone of the chart with 82% of the data in the clay contractive sensitive region and 18% in the clay contractive (CC) region. Points having the highest GH content plot at the limit of the CC region and tend toward a transitional contractive behavior. However, points where GH could not be quantified show a more pronounced trend toward a transitional contractive behavior with high Q_{tn} and U_2 values up to 280 and 70, respectively. No points were detected in the sand dilative region where the pore pressure remains zero during the piezocone penetration and corresponds to the drained region on the original classification chart presented by Schneider et al. (2008). This indicates that the piezocone penetration occurred fully undrained in GH-bearing sediments. On the other hand, the $Q_{tn} - F_r$ chart shows a range of F_r values (0.7 to 8.8) that is almost the same for GH-bearing sites and sites without hydrate. It also suggests a tendency toward a dilative behavior for GH-bearing sediment, with almost 79% of the data plotting between the sand dilative, the transitional dilative

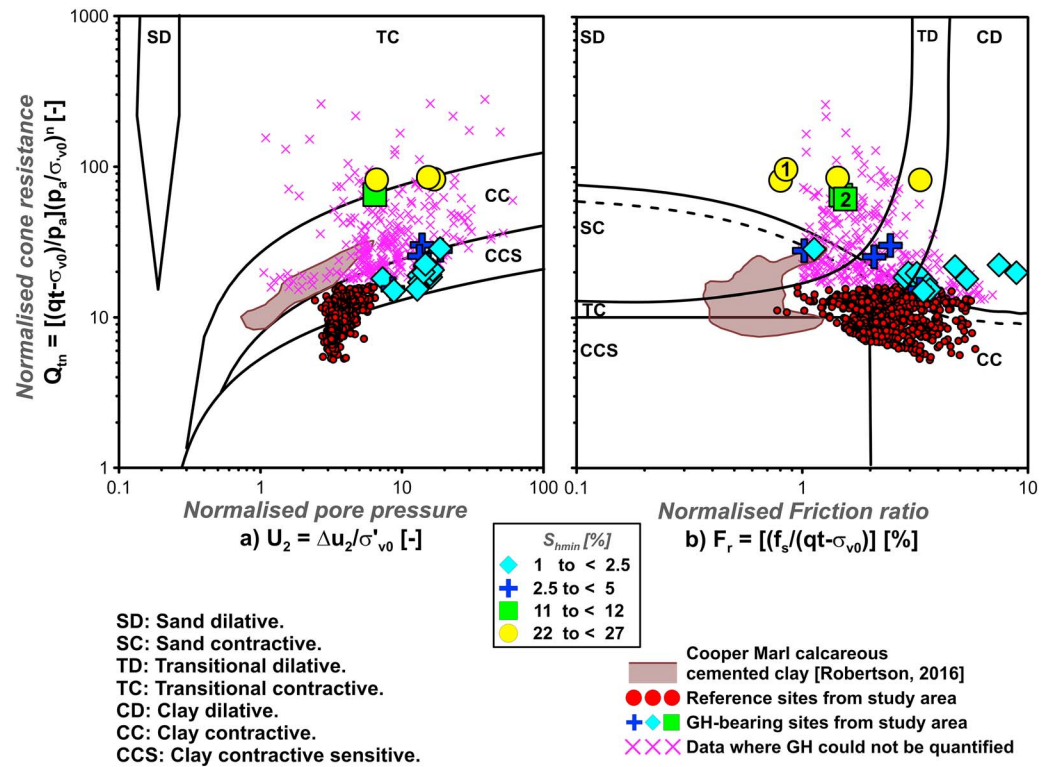


Figure 7. Piezocone data from reference sites (without GH), GH-bearing sites, and calcareous cemented clay (after Robertson, 2016) plotted in: (a) $Q_{tn} - U_2$ chart and (b) $Q_{tn} - F_r$ chart (Robertson, 2016). Data from GH-bearing sites are represented by pink crosses where the GH content could not have been estimated and by different symbols and colors referring to estimates of GH content (i.e., S_{hmin} , see legend).

and the clay dilative regions. However, some points that were classified as CC in the $Q_{tn} - U_2$ chart are also classified as contractive in the $Q_{tn} - F_r$ chart. It is noteworthy that two of these points show a behavior that correlates with the upper limit of Cooper Marl cemented clays on the $Q_{tn} - F_r$ chart, as proposed by Robertson (2016).

4.4. Mechanical Properties of GH-Bearing Sediment

In line with previous observation regarding changes in corrected cone tip resistance (q_t), sleeve friction (f_s), and pore water pressure (Δu_2) in the GH occurrence zone identified by Wei et al. (2015), Figure 8 reveals that the presence of GH has a noticeable effect on the compressibility, stiffness, and strength properties of their host clayey sediments. For instance, the compression indices (λ), the shear moduli at 50% mobilized strength (G_{50}), and the undrained shear strengths (S_u) in the GH-bearing sediment do not follow the linear trends exhibited by the reference sediment. The compression indices (λ) are constantly lower in the GH occurrence zone with values 20 to 40 times lower than those estimated at equivalent depths at the reference site (GMPFM06S01). Away from those spikes, λ values are about 3 to 4 times lower in the GH-bearing sediment.

Increases in stiffness seem less significant with G_{50} values being 1.25 to 7 times higher in GH-bearing sediments compared to sediments without GH (Figure 8).

The increases in undrained shear strength mimic the increases in stiffness, though GH-bearing sediments are up to 25 times stronger than reference sediments where spikes are observed and 2 to 3 times stronger away from the spikes (Figure 8). The fact that the stiffness and strength of GH-bearing sediments vary simultaneously explains why their rigidity indices ($I_r = G_{50}/S_u$) do not remarkably differ from those of sediments without hydrate (Figure 8). By contrast, with the noticeable changes in compressibility, stiffness, and strength, the sensitivity does not appear to be affected by the presence of hydrate (Figure 8).

Plots of geotechnical properties derived from piezocone data against GH content shown in Figure 9 suggest that the compressibility of GH-bearing clayey sediment follows two distinct trends. The first trend may be

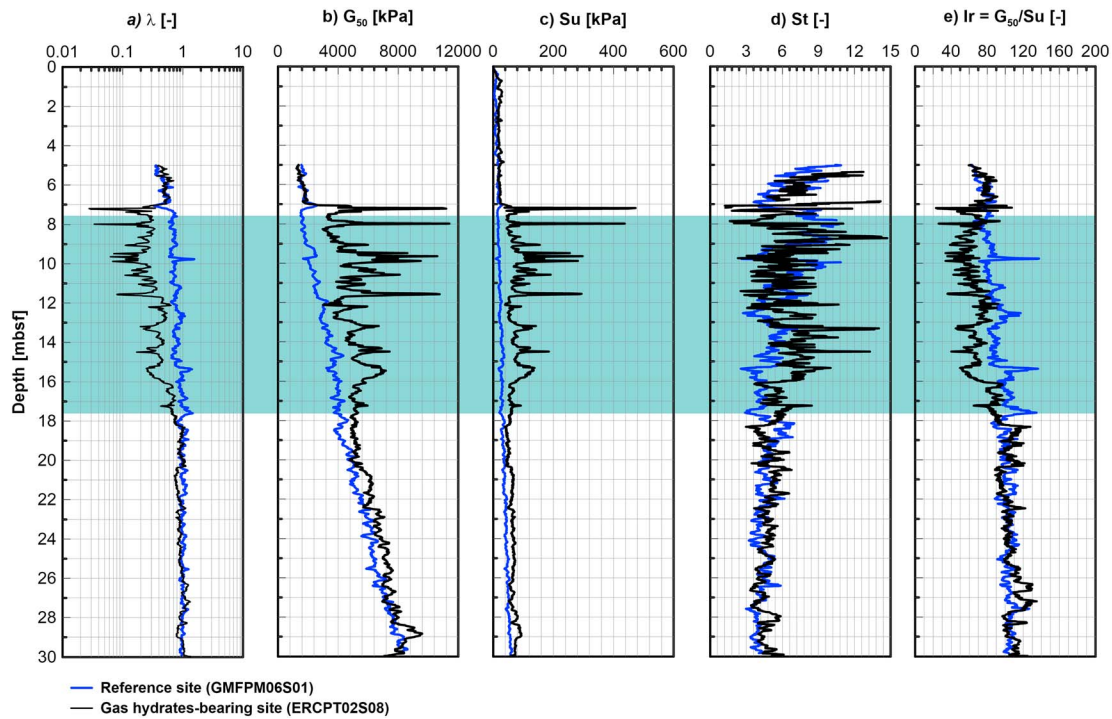


Figure 8. Depth profiles of geotechnical properties derived from piezocone data from the reference site GMFPM06-01 (blue), and the GH-bearing site ERCPT02-08 (black): a. compression index, λ ; shear modulus at 50% mobilized strength, G_{50} , undrained shear strength, S_u ; sensitivity, St ; rigidity index, I_r . The light blue rectangle shows the GH occurrence zone identified by Wei et al., (2015) from chloride anomalies and infrared images.

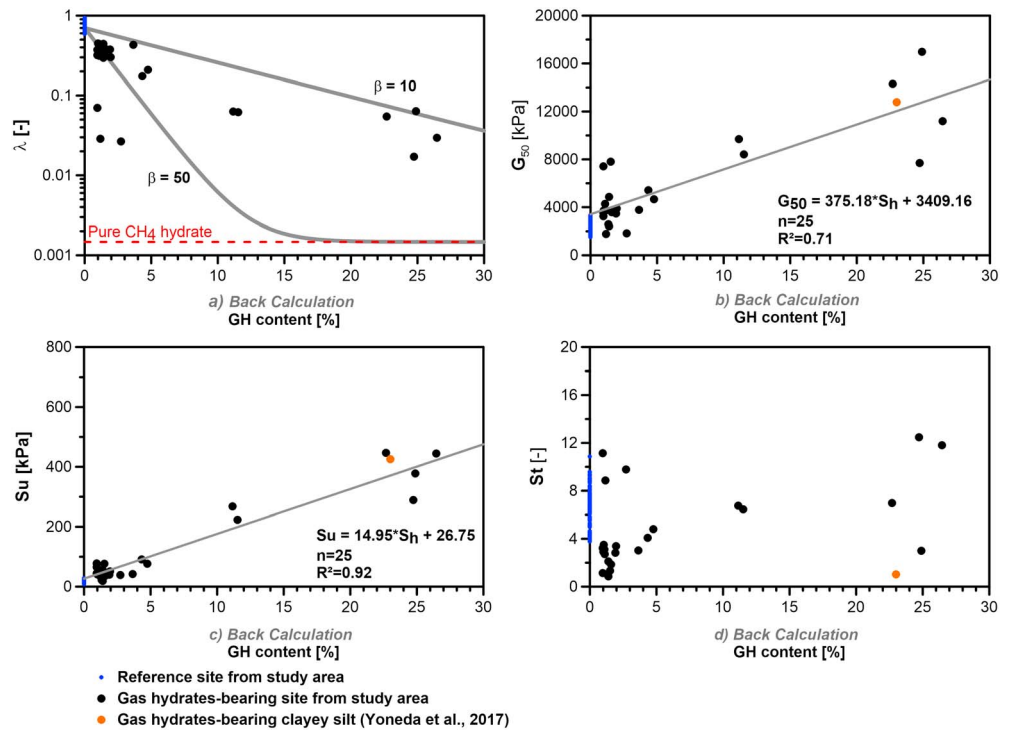


Figure 9. Plots of geotechnical properties derived from piezocone data against hydrate content, S_h estimated from nearby acoustic soundings: (a) compression index, λ ; (b) shear modulus at 50% mobilized strength, G_{50} ; (c) undrained shear strength, S_u , (d) sensitivity, St . hydrate-free sediments are plotted for reference as blue dots. The orange dots in (b–d) are determined from the results of triaxial compression tests on natural, never depressurized gas hydrate (GH)-bearing clayey silt samples from the eastern Nankai trough as reported by Yoneda et al. (2017).

defined by values of compression indices decreasing from 0.47 to 0.026 for values of S_h increasing from 0.94% to 2.76%. The second one outlines a softer decrease in compressibility with GH content with λ reaching 0.06 to 0.017 for S_h values ranging from 22.7% to 26.5%. Values of shear moduli at 50% mobilized strength (G_{50}) appear to follow a more linearly increasing trend with S_h despite some scatter at low and high S_h (Figure 9). With a regression coefficient R^2 of 0.92, values of undrained shear strength follow a linear increase with increasing S_h . By contrast, no clear trend can be observed when plotting values of sensitivity against S_h . Sensitivities around 7 are indeed associated with S_h ranging from 0.94% to 22.7%.

4.5. Hydraulic Properties of GH-Bearing Sediment

Figure 10 shows the initial excess pore pressure pulse (U_{ini}) and dissipation generated by the piezometer penetration during a maximum time-period of 64 hr from different depths at sites GMPZ2, 3, 4, 6, 7, and 10 (for location see Figure 1). Data in Figure 10 were arbitrarily subdivided into two classes: (1) High initial excess pore pressure pulse ($U_{ini} > 150$ kPa) and (2) low initial excess pore pressure pulse ($U_{ini} < 150$ kPa).

Following Burns and Mayne (1999), sediments with a dilative behavior are characterized by Δu curves increasing with time to a certain maximum and then decreasing to in situ equilibrium pore water pressure. In this study, Δu curves are observed to decrease in a monotonic way with time, which is indicative of a contractive behavior as described by Burns and Mayne (1999).

Figure 11 shows $\frac{C_h}{\sqrt{I_r}}$ and U_{ini} as a function of the corrected tip resistance q_t obtained from CPTu testing carried out near the piezometer sites. The clear increase of U_{ini} with q_t for the two reference sites as well as for sites with GH confirms the dependency of U_{ini} on the mechanical properties of the sediments. In effect, U_{ini} is the result of a mean normal octahedral stress (Δu_n) caused by the displacement of the sediment and fluid by the penetrating rod and the shear stress generated at the sediment-rod interface (Δu_{shear}) (Burns & Mayne, 1998).

The $\frac{C_h}{\sqrt{I_r}}$ values obtained from the two reference sites indicate a decrease of this normalized parameter with the increase of q_t (Figure 11). However, $\frac{C_h}{\sqrt{I_r}}$ values for GH-bearing sediments did not show any tendency to increase with q_t . Such result is unusual since the $\frac{C_h}{\sqrt{I_r}}$ values are expected to be proportional to the permeability of the medium and therefore to decrease with the increase of GH content and the increase of q_t .

Figure 12 shows $\frac{C_h}{\sqrt{I_r}}$ as a function of GH content S_h derived from the chloride data and in situ Vp measurements. It can be observed that $\frac{C_h}{\sqrt{I_r}}$ decreases to a minimum value for S_h equal to 10% and then increases again. However, considering the small change of the rigidity index I_r with S_h (Figure 8), it is obvious that the tendency of hydraulic diffusivity to decrease with increasing GH content is not confirmed by the present in situ pore pressure measurements.

5. Discussion

5.1. Quantification and Characterization of GH

In this study, the presence of GH within fine-grained marine sediment have been characterized based on in situ geotechnical and acoustic measurements. The presence of GH was linked to positive Vp anomalies that correlate with an increase in all of the CPTu parameters. However, negative Vp anomalies were indicators of the presence of free gas. The effective medium theory developed by Helgerud et al. (1999) was used to obtain an upper- and lower-bound estimate of GH content within the sediment based on compressional wave velocity anomalies.

Comparisons of velocity-derived estimates were made with those derived from pore water chloride anomalies to evaluate which of the upper- or lower-bound GH content might be more reliable to use in the study area. It was found that S_{hmin} values are fairly close to those derived from pore water chloride analyses. These observations are in line with studies performed by Ghosh et al. (2010), in which it was shown that S_{hmin} yields closer estimates to that of the pressure core depressurization method compared to S_{hmax} . Hence, for this paper S_{hmin} was used to carry out the investigation of the effect of GH content on the

mechanical and hydraulic properties of the host sediment. In general, no systematic vertical pattern was noticed on the GH profiles (Figure 6).

Wei et al. (2015) discussed GH distribution in the study area based on cold temperatures obtained from infrared imaging. Therefore, negative thermal anomalies derived from MeBo cores by Wei et al. (2015) were compared to GH occurrence zones determined using the effective medium theory. Both methods showed close results by exhibiting almost the same GH occurrence zone; therefore, confirming the relation between Vp anomalies and the presence of hydrates.

Using the effective medium theory, a maximum GH content of 26.5% (S_{hmin}) was estimated to correlate with a Vp of 2,035 m/s. Because of the limitation of the ultrasonic fork, which can only measure Vp up to 2,200 m/s, higher GH content could not have been estimated.

The estimation of GH content might have been also affected by the coexistence of free gas and solid GH in the study area as reported by Sultan et al. (2007, 2010). This phenomenon is mainly caused by the fact that the study area is characterized by a high gas flux system; hence, in some cases free gas can be isolated within the pores of GHs where no water is available for the formation of solid hydrates; resulting in a GH containing voids and having a spongy texture. It is indeed thought that GH content might have been locally underestimated when the presence of free gas could have counteracted the effect of hydrates in increasing Vp.

Soil classification charts were used to define a general trend that illustrates the behavior of GH-bearing clayey sediments by correlating in situ acoustic data with geotechnical properties. While the highest GH content correlates with the highest U_2 and Q_{tn} values, the rest of the data do not bear a proportional relationship with hydrate content. However, GH-bearing sediments are clearly characterized by slightly increasing U_2 values that correlate with large Q_{tn} values (compared to reference sites), which reflect a contractive behavior. These observations are in contrast with results from laboratory triaxial experiments performed on GH-bearing sandy sediments, where the behavior was found to be significantly dilative at high GH content (Hyodo et al., 2013). Interestingly, Liu et al. (2018), showed that upon shearing the dilatancy of GH-bearing sands is higher compared to that of GH-bearing silts. Moreover, data from sites where GH content could not have been estimated show a general trend of increasing Q_{tn} values toward the upper limit of the charts. This confirms that GH contribute to the increase of the stiffness and strength of their host sediment. However, the fact that no clear trend of increasing U_2 with increasing Q_{tn} can be discerned tends to suggest that the sensitivity of GH-bearing sediments does not increase proportionally to their stiffness and strength. This suspicion is supported by the analysis of the $Q_{tn} - F_r$ chart, which reveals that high values of Q_{tn} correlate with values of F_r varying over a wide range. The combination of $Q_{tn} - U_2$ and $Q_{tn} - F_r$ charts also reveals that data from GH-bearing sites tend to plot in different regions.

While, the $Q_{tn} - F_r$ chart suggests a dilative behavior for most of the data, the $Q_{tn} - U_2$ chart reflects a contractive behavior. Robertson (2016) suggested that such a difference is representative of the influence of the increasing microstructure in in situ soils. Here the difference between both classification charts can be explained by the increasing GH content within the sediment. By contrast, for some data points, the behavior is classified as contractive in both charts.

These findings can be explained with reference to different GH concentrations and morphologies accommodated by clayey sediments. Visual observations of recovered cores in the study area show GH morphologies varying from groups of millimeter-thick veins to massive nodules (Sultan et al., 2010). Correlations of these observations with the acoustic and geotechnical data show high GH concentrations (up to 27%) plotting in the dilative region of the $Q_{tn} - F_r$ chart, which could be related to the presence of nodule type hydrate. However, low GH concentrations (1% to 5%) plotting in or at the limit of the contractive region of the $Q_{tn} - F_r$ chart could be an indicator of the presence of a group of hydrate veins.

Alternatively, Ramsey (2010) discussed that the presence of massive inclusion (i.e., GH nodules in this study) within the sediment might influence piezocone response. This can eventually lead to local suction that prevent the proper functioning of the pore pressure sensor, therefore, producing sharp drops in pore water pressure data correlating with spikes in the f_s profile. Such a response has been observed twice during this analysis (symbols 1 and 2 on Figure 7) for GH content of 26.5% and 11.5%, respectively. During the penetration, Δu_2 did not reduce below -70 kPa confirming that it did not drastically affect the reliability of the measuring method.

5.2. Mechanical Properties of GH-Bearing Sediment

The derivation of geotechnical properties from piezocone data allowed estimating the extents to which the presence of GH tend to decrease the compressibility of clayey sediments while increasing their stiffness and strength (Figures 8 and 9). Keeping in mind that empirical correlations primarily defined for *ideal soils* have been used to derive these properties and that there are difficulties inherent to the estimation of GH content, the trends that emerged are cautiously discussed here. A common feature to the compression index, shear modulus, and undrained shear strength is to show a wide scatter with S_h ranging from 0.94% to 3%. In the lack of laboratory results to substantiate these observations, one may suspect that the morphology and orientation of grain-displacing hydrate readily take over from S_h as the primary control of the compressibility, stiffness, and strength. Following Ghosh et al. (2010) one may also infer that the orientation of grain-displacing hydrate affects the estimation of GH content (S_h) using an effective medium theory approach.

Values of compression indices can be compared to the model proposed by Sultan et al., (2010) to capture the evolution of compressibility with S_h . According to this empirical model, compression indices of GH-bearing sediments (λ_h) are expected to asymptotically decrease from a value typical of purely water-saturated sediments in the study area ($\lambda_0 = 0.7$) toward that of pure hydrate ($\lambda_1 = 0.00147$) according to the following equation:

$$\lambda_h = \lambda_0 \left[1 - \left(1 - \left(\frac{\lambda_1}{\lambda_0} \right) \right) \left(1 - \exp \left(-\beta \cdot \frac{S_h}{100} \right) \right) \right] \quad (12)$$

Where the coefficient β is expected to reflect the distribution and morphology of GH within the sediment.

As shown in Figure 9, a β value of 10 appears to provide an upper limit for the compression indices of GH-bearing sediments. It would predict that the compressibility of the host sediments approaches that of pure methane hydrate for $S_h = 100\%$. A β value of 50 would provide a lower limit for the compression indices of most of the GH-bearing sediments. The fact that it implies that the compressibility of GH-bearing sediments approaches that of pure methane hydrate for $S_h = 18\%$ can hardly be reconciled with the data showing that when S_h is in the range 25–27%, compression indices remain 1 order of magnitude higher than that of pure GH. This raises the possibility that a single β value cannot capture the change in compressibility with S_h as the morphology of GH is itself evolving with S_h . Thus, the identification of robust trends from laboratory testing of natural, fine-grained GH-bearing sediments is required to expand upon this empirical suspicion.

Despite some scatter in the plots of Figure 9b, the overall distribution suggests that the stiffness and strength of GH-bearing clayey sediments tend to increase linearly with S_h . The fact that S_u data appear less scattered than the G_{50} data may be ascribed to the fact that the latter have been calculated using the soil behavior type index (I_c), whose calculation may be affected by a lack of accuracy of sleeve friction measurements, f_s (see section 3.4). An additional note of caution has to do with the fact that density was assumed to be constant when calculating G_{50} . One may however note that the unique natural GH-bearing fine-grained sediments subjected to triaxial compression by Yoneda et al. (2017) has G_{50} and S_u values falling close to the linear trends that emerged from the present study. As for compression indices, it can be expected that the stiffness and strength is influenced by the distribution and morphology of GH such that S_h alone cannot wholly capture the natural variability of these properties.

Sensitivity values are discussed separately from the previous properties as they appear to be the most scattered when plotted against S_h . Such a scatter might be attributed to a lack of accuracy of sleeve friction measurements. However, the plots in the $Q_{tn} - U_2$ chart in Figure 7a, which do not rely on sleeve friction measurements, also suggest that sensitivity bears little relationship to S_h . Indeed, values of Q_{tn} ranging from 11 to 80 are observed to display similar U_2 values for S_h ranging from less than 2.5% to more than 22%, while sensitive sediments are expected to display trends of increasing Q_{tn} with increasing U_2 (Robertson, 2016).

In line with previous interpretations, this tend to support the view that the distribution and morphology of GH have a strong influence on sensitivity.

5.3. Hydraulic Properties of GH-Bearing Sediment

The water permeability of GH-bearing sediments is a constraint for reservoir engineering studies but, moreover, a key parameter to evaluate the excess pore pressure generated by hydrate decomposition in natural environment.

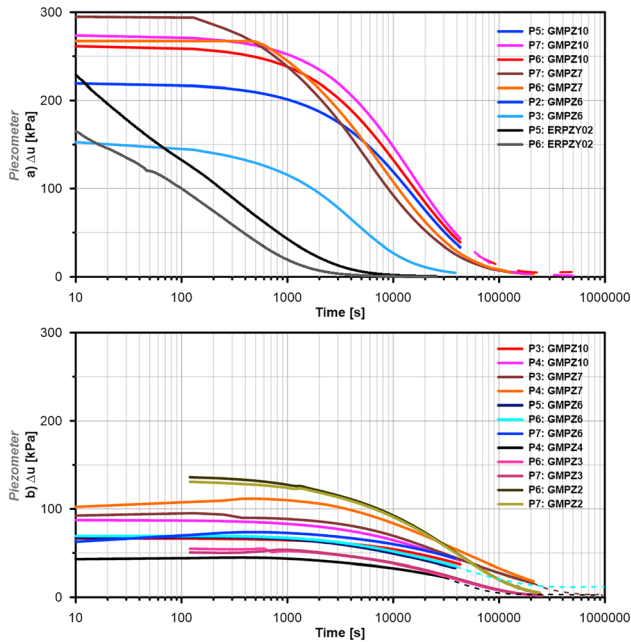


Figure 10. Pore pressure dissipation curves from different depths at different sites (GMPZ2, 3, 4, 6, 7, and 10) where the presence of GH was suspected and/or proved. Panels (a) and (b) show data where the initial excess pore pressure pulse (U_{ini}) values are higher and lower than 150 kPa. When the excess pore pressure was not equilibrated at the end of the deployment, the extrapolation of the excess pore pressure was carried out using the numerical algorithm developed by Sultan and Lafuerza (2013; dashed lines).

The evolution of the octahedral stress (Δu) with time is a means to predict if the investigated soil is contractive or dilative. Pore pressure dissipation curves from different piezometer sites have indeed showed a monotonic change with time. This trend is representative of a contractive behavior as proposed by Burns and Mayne (1999); thus confirming what has been observed in section 5.1 for GH-bearing clayey sediments.

The rare available data from literature are often obtained from laboratory experimental tests carried out on reconstructed GH-bearing sand samples. Those laboratory data show a clear tendency of the permeability to decrease with increasing GH content (see, for instance, Katagiri et al., 2017, and references therein). On the other hand, different authors show that the water permeability versus porosity of the hydrate-sediment system depends on the way GH accommodates the pore spaces (grain coating or pore filling). Several theoretical models were developed in the recent years in order to define the link between GH content and relative permeability (Katagiri et al., 2017; Kleinberg et al., 2003; Moridis, 2002, among others).

Kleinberg et al. (2003) have summarized existing expressions for the relative permeability k_{hw} in hydrate-bearing sediment. For pore-filling hydrate, a simple relative permeability to water can be expressed by the following expression:

$$k_{hw} = \frac{k}{k_0} = \frac{(1 - S_h)^{m+2}}{(1 + \sqrt{S_h})^2} \quad (13)$$

where k_0 is the reference permeability of the saturated sediment, k is the permeability of the system for a given hydrate saturation, and m is the saturation exponent decreasing from 0.4 for $S_h = 10\%$ to 0.1 in a fully hydrate saturated system. For grain-coating hydrate, a simple expression of the relative permeability to water is given by

$$k_{hw} = \frac{k}{k_0} = (1 - S_h)^{m+1} \quad (14)$$

where $m = 1.5$ for $S_h < 80\%$.

Before discussing changes in relative permeability to water, attention is paid to the changes in relative hydraulic diffusivity with GH content from in situ measurements:

$$C_{hw} = \frac{C_h}{C_{h0}} \quad (15)$$

where C_h is the hydraulic diffusivity of the system for a given hydrate content and C_{h0} is the reference hydraulic diffusivity of the saturated sediment.

The C_{hw} values shown in Figure 13a are derived from piezometer data in Figure 12 and the rigidity indices (I_r) obtained from CPTu data using the Robertson (2009) method (Figure 8). The plots in Figure 13a confirm the decreasing trend of C_{hw} with increasing S_h up to 15%. However, a clear increase of C_{hw} with S_h can be observed for S_h values higher than 20%. Such results were unexpected and were initially considered as erroneous data, compromising the used in situ method to determine the hydraulic properties of GH-bearing sediments. However, published experimental data and models often consider the sediment hydrate medium as a

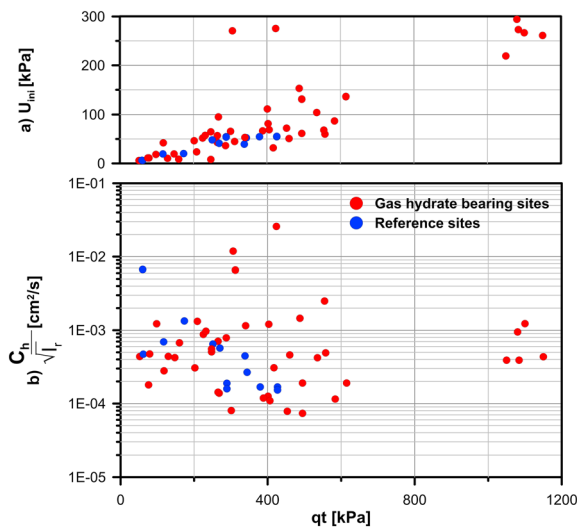


Figure 11. (a) U_{ini} and (b) $\frac{C_h}{\sqrt{I_r} \sqrt{L}}$ as a function of q_t showing a strong dependence of the initial excess pore pressure pulse on the corrected tip resistance. The $\frac{C_h}{\sqrt{I_r} \sqrt{L}}$ values do not show any clear tendency.

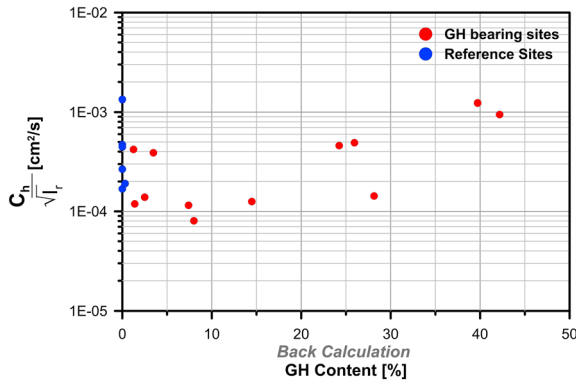


Figure 12. $\frac{C_h}{\sqrt{t_r}}$ as a function of GH content (S_h). $\frac{C_h}{\sqrt{t_r}}$ decreases to a minimum value for S_h equal 10% and then increases again.

continuous system without discontinuities and fractures. In natural environments, the presence of fractures at different scales may imply high hydraulic diffusivities and fluid flows paths through GH-bearing areas. The coexistence of free gas and GH as well as gas plumes in the water column above hydrate occurrence zones is a clear evidence of the presence of these discontinuities (Riboulot et al., 2018; Sauter et al., 2006; Torres et al., 2004). The impact of those discontinuities on the evolution of the hydraulic diffusivity with the GH content seems essential to account for accurate prediction of fluid flow through hydrate-sediment systems. The use of in situ pore pressure measurements and the pore pressure decay with time to derive the hydraulic diffusivity of the medium looks, at first sight, as a reliable method to access the in situ hydraulic properties of sediment-hydrate fracture mediums. Therefore, our data importantly suggest that, in the study area, fractures occurring for S_h values higher than 20% may drastically increase the hydraulic diffusivity of the GH-bearing sediments. Unfortunately, this strong conclusion is premature, since alternative explanation related either to the piezometer installation or to the important decrease of the compressibility could also be at the origin of the increase in C_{hw} with S_h . The free-fall method used for piezometer installation with a rod diameter of 0.06 m and the stiffness of the GH-bearing sediments could enhance fracture propagation or even initiation. The expected consequence would be an increase in hydraulic diffusivity. Although, fractures generated by piezometer penetrations are more likely to occur at the tip of the piezometer and not all over its shaft (Santamarina et al., 2015), at this stage, it is not possible to firmly conclude about their origin. However, it is obvious that the general thought about the decrease of the hydraulic diffusivity with increasing hydrate content cannot be systematically applied in natural sediment-hydrate systems.

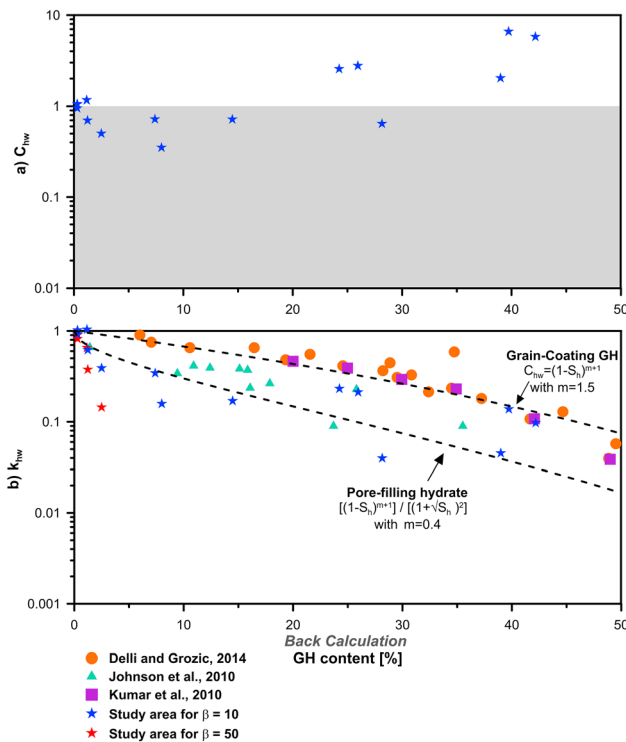


Figure 13. (a) Relative hydraulic diffusivity (C_{hw}) as a function of hydrate content (S_h) showing a decrease tendency with the increase of S_h to 15%. A clear increase of C_{hw} with S_h can be observed for S_h values higher than 20%. (b) Relative permeability data for β values of 10 and 50.

To further the discussion, it is important to mention that the hydraulic diffusivity is equal to the relative permeability to water divided by the storage parameter:

$$k_{hw} = \frac{k}{k_0} = \frac{C_h \cdot St_h}{C_{h0} \cdot St_0} = C_{hw} \cdot \frac{\gamma_w \cdot m_{vh}}{\gamma_w \cdot m_{v0}} = C_{hw} \cdot \frac{\lambda_h}{\lambda_0} = C_{hw} \left[1 - \left(1 - \left(\frac{\lambda_1}{\lambda_0} \right) \right) \left(1 - \exp \left(-\beta \cdot \frac{S_h}{100} \right) \right) \right] \quad (16)$$

Where St_0 and St_h are storage factors, γ_w is the water unit weight, and m_{v0} and m_{vh} are the volume compressibility coefficients of water-saturated and hydrate-bearing sediments, respectively. As shown in Table 3 and Figure 13, values of relative permeability to water (k_{hw}) can be calculated using equation (16), assuming upper and lower β values of 10 and 50 as explained in section 5.2. However, since for $S_h > 5\%$ no data plot near the limit curve obtained using a $\beta = 50$ (Figure 9a), k_{hw} values were calculated using $\beta = 50$ only for values of $S_h < 5\%$.

Figure 13b shows that overall the calculated k_{hw} data decrease with increasing S_h . This trend reflects the fact that the compressibility of GH-bearing sediments decreases more rapidly than the hydraulic diffusivity does with increasing S_h . The k_{hw} values obtained with β values of 10 generally plot between the two limit curves defined by equations (13) and (14) while showing a decreasing trend with increasing S_h . While these equations were developed for coarse-grained sediments, they appear here to have the potential to serve as lower and upper bounds for describing the evolution of permeability as a function of hydrate content in clayey sediments also. On the other hand, for $\beta = 50$, k_{hw} data plot completely outside of the grain-coating and pore-filling hydrate limits

Table 3
Hydraulic Properties From Different Depths at Different Sites (GMPZ2, 3, 4, 6, 7, and 10) Where the Presence of Gas Hydrate Was Suspected and/or Proved

Site	Depth (mbsf)	t_{50} (s)	S_h (%)	C_h (m ² /s)	C_{hw}	k_{hw} for $\beta = 10$	k_{hw} for $\beta = 50$
GMPZ2	7.08	23686	0.3	2.23E-07	0.951	0.923	0.819
GMPZ2	7.11	23686	0.3	2.46E-07	1.049	1.018	0.904
GMPZ3	7.11	28347	1.16	2.72E-07	1.161	1.034	0.651
GMPZ4	6.17	31550	28.15	1.51E-07	0.642	0.040	
GMPZ4	6.97	9806	24.2375	5.99E-07	2.555	0.231	
GMPZ4	7.005	9183	25.95	6.47E-07	2.761	0.211	
GMPZ6	6.98	10715	1.24	1.64E-07	0.698	0.616	
GMPZ7	6.23	32546	2.5	1.17E-07	0.500	0.390	
GMPZ7	7.78	35944	14.475	1.68E-07	0.716	0.169	
GMPZ7	10.13	3668	39.725	1.55E-06	6.591	0.138	
GMPZ7	10.165	4766	42.175	1.36E-06	5.787	0.097	
GMPZ10	6.93	56169	8	8.22E-08	0.350	0.158	
GMPZ10	8.48	39219	7.4	1.68E-07	0.718	0.343	
GMPZ10	10.03	11574	38.9875	4.75E-07	2.025	0.045	

(equations (13) and (14)) while decreasing with a slope 14 times steeper than that of the k_{hw} obtained with $\beta = 10$. This implies that the trends defined by equations (13) and (14) are clearly not adapted to represent the evolution of k_{hw} calculated with β values of 50. This highlights the need for developing new models that can account for the evolution of the morphology of GH with that of S_h .

6. Conclusion

The main objective of this work was to study the effect of GH concentration and morphology on the mechanical and hydraulic properties of their host clayey sediment. This was achieved by using a unique database containing multiple in situ acoustic, geotechnical, coring, and drilling data. This investigation allowed capturing the behavior of clayey sediment with GH content varying between 1% and 26.5% in a high gas flux system in the Gulf of Guinea. This analysis led to the following key observations:

1. Positive V_p anomalies correlating with simultaneous increase of all geotechnical parameters (q_v , f_s , and Δu_2) are indicative of the presence of GH.
2. Using the effective medium theory, a maximum GH content of 26.5% was estimated to correlate with a V_p of 2,035 m/s.
3. Comparisons of results derived from the effective medium theory with those derived from negative thermal anomalies yielded almost the same GH occurrence zone.
4. GH-bearing clayey sediments generally show a contractive behavior, which was confirmed by the analysis of pore pressure dissipation data recorded by piezometers. Such a behavior contrasts sharply with the dilative behavior of GH-bearing sandy sediments.
5. Results have shown that the normalized piezocone resistance (Q_{tn}) increases with the GH content. High Q_{tn} values were found to correlate with the same range of U_2 values. This suggests that the morphology and the distribution of GH has an important effect on the mechanical properties of the host sediment.
6. The use of different soil behavior classification charts, while carefully analyzing all used parameters, might be a means to identify different GH morphologies based on zones in which the piezocone data plot.
7. The presence of GH has a noticeable effect on the compressibility, stiffness, and strength properties of their host clayey sediments. It tends to increase the stiffness G_{50} and undrained shear strength (S_u) while decreasing the compressibility. While no clear trend was observed between the sensitivity and GH content, S_u and G_{50} appear to follow a linear increase with GH content.
8. Oscillations around the linear trend are thought to reflect the superimposed influence of the distribution and morphology of GH on the stiffness and strength.
9. Pore pressure dissipation data were used to derive the relative hydraulic diffusivity (C_{hw}) as a function of hydrate content (S_h). At low hydrate content, C_{hw} was observed to decrease with increasing S_h . For S_h

values higher than 20, C_{hw} values rising above 1 were linked either to the presence of fractures in the hydrate-sediment system or to the important decrease of compressibility with increasing GH content. This observation leads to the conclusion that the pore pressure diffusion within GH systems could be much faster than previously thought for high hydrate content.

Further investigations supported by experimental data would be helpful in substantiating the influence of various morphologies and amount of GH on the mechanical and hydraulic properties of the clayey host sediment.

Acknowledgments

Data used in the present paper are covered by a confidentiality agreement between Total, Ifremer, and Marum that restrict access; interested readers can contact the authors for more information. Sandrine Cheron from Ifremer is thanked for her assistance in performing mineralogical analyses. The authors would like to express their great appreciation to the French National Research Agency for funding the present study, which is part of the project HYDRE "Mechanical behavior of gas-hydrate-bearing sediments" – ANR-15-CE06-0008.

References

- ASTM Standard D2435 (1996). Standard TEST method for one-dimensional consolidation properties of the soil, ASTM International, West Conshohocken, PA 19428, www.astm.org.
- Boswell, R., & Collett, T. (2006). The gas hydrate resource pyramid. *Natural Gas & Oil*, 304, 285–4541.
- Boswell, R., & Collett, T. S. (2011). Current perspectives on gas hydrate resources. *Energy & Environmental Science*, 4(4), 1206–1215. <https://doi.org/10.1039/C0EE00203H>
- Burns, S., & Mayne, P. (1999). Pore pressure dissipation behaviour surrounding driven piles and cone penetrometers. *Transportation Research Record: Journal of the Transportation Research Board*, 1675, 17–23. <https://doi.org/10.3141/1675-03>
- Burns, S. E., & Mayne, P. W. (1998). Monotonic and dilatatory pore-pressure decay during piezocone tests in clay. *Canadian Geotechnical Journal*, 35(6), 1063–1073. <https://doi.org/10.1139/t98-062>
- Cunningham, R., & Lindholm, R. M. (2000). AAPG memoir 73, Chapter 8: Seismic evidence for widespread gas hydrate formation, offshore West Africa.
- Dai, S., Santamarina, J. C., Waite, W. F., & Kneafsey, T. J. (2012). Hydrate morphology: Physical properties of sands with patchy hydrate saturation. *Journal of Geophysical Research*, 117, B11205. <https://doi.org/10.1029/2012JB009667>
- Freudenthal, T., & Wefer, G. (2007). Scientific drilling with the sea floor drill rig MeBo. *Scientific Drilling*, 5, 63–66. <https://doi.org/10.5194/sd-5-63-2007>
- Freudenthal, T., & Wefer, G. (2013). Drilling cores on the sea floor with the remote-controlled sea floor drilling rig MeBo. *Geoscientific Instrumentation, Methods and Data Systems*, 2(2), 329–337. <https://doi.org/10.5194/gi-2-329-2013>
- Ghosh, R., Sain, K., & Ojha, M. (2010). Effective medium modeling of gas hydrate-filled fractures using the sonic log in the Krishna-Godavari basin, offshore eastern India. *Journal of Geophysical Research*, 115, B06101. <https://doi.org/10.1029/2009JB006711>
- Helgerud, M. B., Dvorkin, J., Nur, A., Sakai, A., & Collett, T. (1999). Elastic-wave velocity in marine sediments with gas hydrate: Effective medium modeling. *Geophysical Research Letters*, 26(13), 2021–2024. <https://doi.org/10.1029/1999GL900421>
- Hovland, M., Gallagher, J. W., Clennell, M. B., & Lekvam, K. (1997). Gas hydrate and free gas volumes in marine sediments: Example from the Niger Delta front. *Marine and Petroleum Geology*, 14(3), 245–255. [https://doi.org/10.1016/S0264-8172\(97\)00012-3](https://doi.org/10.1016/S0264-8172(97)00012-3)
- Hyodo, M., Yoneda, J., Yoshimoto, N., & Nakata, Y. (2013). Mechanical and dissociation properties of methane hydrate-bearing sand in deep seabed. *Soils and Foundations*, 53(2), 299–314. <https://doi.org/10.1016/j.sandf.2013.02.010>
- Jang, J., & Santamarina, J. C. (2016). Hydrate bearing clayey sediments: Formation and gas production concepts. *Marine and Petroleum Geology*, 77, 235–246. <https://doi.org/10.1016/j.marpetgeo.2016.06.013>
- Katagiri, J., Konno, Y., Yoneda, J., & Tenma, N. (2017). Pore-scale modeling of flow in particle packs containing grain-coating and pore-filling hydrate: Verification of a Kozeny–Carman-based permeability reduction model. *Journal of Natural Gas Science and Engineering*, 45, 537–551. <https://doi.org/10.1016/j.jngse.2017.06.019>
- Kayen, R. E., & Lee, H. J. (1991). Pleistocene slope instability of gas hydrate-laden sediment on the Beaufort Sea margin. *Marine Georesources & Geotechnology*, 10(1–2), 125–141. <https://doi.org/10.1080/10641199109379886>
- Kleinberg, R. L., Flaum, C., Griffin, D. D., Brewer, P. G., Malby, G. E., Peltzer, E. T., & Yesinowski, J. P. (2003). Deep sea NMR: Methane hydrate growth habit in porous media and its relationship to hydraulic permeability, deposit accumulation, and submarine slope stability. *Journal of Geophysical Research*, 108(B10), 2508. <https://doi.org/10.1029/2003JB002389>
- Krage, C. P., Broussard, N. S., & DeJong, J. T. (2014). Estimating rigidity index (IR) based on CPT measurements. In *Third international symposium on cone penetration testing, Las Vegas, Nevada, USA* (pp. 727–735). Las Vegas, NV.
- Kvenvolden, K. A. (1993). Gas hydrate as a potential energy resource—A review of their methane content. United States Geological Survey, *Professional Paper; (United States)*, 1570.
- Liu, Z., Dai, S., Ning, F., Peng, L., Wei, H., & Wei, C. (2018). Strength estimation for hydrate-bearing sediments from direct shear tests of hydrate-bearing sand and silt. *Geophysical Research Letters*, 45, 715–723. <https://doi.org/10.1002/2017GL076374>
- Low, H. E., Lunne, T., Andersen, K. H., Sjørnsen, M. A., Li, X., & Randolph, M. F. (2010). Estimation of intact and remoulded undrained shear strengths from penetration tests in soft clays. *Géotechnique*, 60(11), 843–859. <https://doi.org/10.1680/geot.9.P.017>
- Lunne, T., Robertson, P. K., & Powell, J. J. M. (1997). Cone penetration testing. *Geotechnical Practice*, 20, 23–35.
- Malinverno, A., Kastner, M., Torres, M. E., & Wortmann, U. G. (2008). Gas hydrate occurrence from pore water chlorinity and downhole logs in a transect across the northern Cascadia margin (Integrated Ocean drilling program expedition 311). *Journal of Geophysical Research*, 113, B08103. <https://doi.org/10.1029/2008JB005702>
- Moridis, G. J. (2002). Numerical studies of gas production from methane hydrate. In *SPE Gas Technology Symposium*. Calgary Alberta, Canada: Society of Petroleum Engineers.
- Ning, F., Yu, Y., Kjelstrup, S., Vlught, T. J., & Glavatskiy, K. (2012). Mechanical properties of clathrate hydrates: Status and perspectives. *Energy & Environmental Science*, 5(5), 6779–6795. <https://doi.org/10.1039/c2ee03435b>
- Paul, C. K., & Ussler, I. W. (2001). History and significance of gas sampling during DSDP and ODP. *Natural Gas Hydrates: Occurrence, Distribution and Detection*. American Geophysical Union, 124, 53–66. <https://doi.org/10.1029/GM124>
- Ramsey, N. (2010). Some issues related to application of the CPT. In *2nd International Symposium on Cone Penetration Testing, CPT* (Vol. 10). Huntington Beach, CA.
- Riboulot, V., Ker, S., Sultan, N., Thomas, Y., Marsset, B., Scalabrin, C., Ruffine, L., et al. (2018). Freshwater lake to salt-water sea causing widespread hydrate dissociation in the Black Sea. *Nature Communications*, 9(1), 117. <https://doi.org/10.1038/s41467-017-02271-z>
- Robertson, P. K. (2009). Interpretation of cone penetration tests—A unified approach. *Canadian Geotechnical Journal*, 46(11), 1337–1355. <https://doi.org/10.1139/T09-065>

- Robertson, P. K. (2016). Cone penetration test (CPT)-based soil behaviour type (SBT) classification system—An update. *Canadian Geotechnical Journal*, *53*(12), 1910–1927. <https://doi.org/10.1139/cgj-2016-0044>
- Santamarina, J. C., Dai, S., Jang, J., & Terzariol, M. (2012). Pressure core characterization tools for hydrate-bearing sediments. *Scientific Drilling*, *14*, 44–48. <https://doi.org/10.5194/sd-14-44-2012>
- Santamarina, J. C., Dai, S., Terzariol, M., Jang, J., Waite, W. F., Winters, W. J., Nagao, J., et al. (2015). Hydro-bio-geomechanical properties of hydrate-bearing sediments from Nankai trough. *Marine and Petroleum Geology*, *66*, 434–450. <https://doi.org/10.1016/j.marpetgeo.2015.02.033>
- Sauter, E. J., Muyakshin, S. I., Charlou, J. L., Schlüter, M., Boetius, A., Jerosch, K., Damm, E., et al. (2006). Methane discharge from a deep-sea submarine mud volcano into the upper water column by gas hydrate-coated methane bubbles. *Earth and Planetary Science Letters*, *243*(3–4), 354–365. <https://doi.org/10.1016/j.epsl.2006.01.041>
- Schneider, J. A., Randolph, M. F., Mayne, P. W., & Ramsey, N. R. (2008). Analysis of factors influencing soil classification using normalized piezocone tip resistance and pore pressure parameters. *Journal of Geotechnical and Geoenvironmental Engineering*, *134*(11), 1569–1586. [https://doi.org/10.1061/\(ASCE\)1090-0241\(2008\)134:11\(1569\)](https://doi.org/10.1061/(ASCE)1090-0241(2008)134:11(1569))
- Sultan, N., Bohrmann, G., Ruffine, L., Pape, T., Riboulot, V., Colliat, J. L., de Prunelé, A., et al. (2014). Pockmark formation and evolution in deep water Nigeria: Rapid hydrate growth versus slow hydrate dissolution. *Journal of Geophysical Research: Solid Earth*, *119*, 2679–2694. <https://doi.org/10.1002/2013JB010546>
- Sultan, N., Garziglia, S., & Ruffine, L. (2016). New insights into the transport processes controlling the sulfate-methane-transition-zone near methane vents. *Scientific Reports*, *6*(1), 26701. <https://doi.org/10.1038/srep26701>
- Sultan, N., & Lafuerza, S. (2013). In situ equilibrium pore-water pressures derived from partial piezoprobe dissipation tests in marine sediments. *Canadian Geotechnical Journal*, *50*(12), 1294–1305. <https://doi.org/10.1139/cgj-2013-0062>
- Sultan, N., Marsset, B., Ker, S., Marsset, T., Voisset, M., Vernant, A. M., Bayon, G., et al. (2010). Hydrate dissolution as a potential mechanism for pockmark formation in the Niger delta. *Journal of Geophysical Research*, *115*, B08101. <https://doi.org/10.1029/2010JB007453>
- Sultan, N., Voisset, M., Marsset, T., Vernant, A. M., Cauquil, E., Colliat, J. L., & Curinier, V. (2007). Detection of free gas and gas hydrate based on 3D seismic data and cone penetration testing: An example from the Nigerian continental slope. *Marine Geology*, *240*(1–4), 235–255. <https://doi.org/10.1016/j.margeo.2007.02.012>
- Teh, C. I., & Houlsby, G. T. (1991). Analytical study of the cone penetration test in clay. *Geotechnique*, *41*(1), 17–34. <https://doi.org/10.1680/geot.1991.41.1.17>
- Torres, M. E., Wallmann, K., Tréhu, A. M., Bohrmann, G., Borowski, W. S., & Tomaru, H. (2004). Gas hydrate growth, methane transport, and chloride enrichment at the southern summit of hydrate ridge, Cascadia margin off Oregon. *Earth and Planetary Science Letters*, *226*(1–2), 225–241. <https://doi.org/10.1016/j.epsl.2004.07.029>
- Waite, W. F., Santamarina, J. C., Cortes, D. D., Dugan, B., Espinoza, D. N., Germaine, J., Jang, J., et al. (2009). Physical properties of hydrate-bearing sediments. *Reviews of Geophysics*, *47*, RG4003. <https://doi.org/10.1029/2008RG000279>
- Wei, J., Pape, T., Sultan, N., Colliat, J. L., Himmler, T., Ruffine, L., de Prunelé, A., et al. (2015). Gas hydrate distributions in sediments of pockmarks from the Nigerian margin—results and interpretation from shallow drilling. *Marine and Petroleum Geology*, *59*, 359–370. <https://doi.org/10.1016/j.marpetgeo.2014.09.013>
- Yoneda, J., Masui, A., Konno, Y., Jin, Y., Kida, M., Katagiri, J., Nagao, J., et al. (2017). Pressure-core-based reservoir characterization for geo-mechanics: Insights from gas hydrate drilling during 2012–2013 at the eastern Nankai trough. *Marine and Petroleum Geology*, *86*, 1–16. <https://doi.org/10.1016/j.marpetgeo.2017.05.024>
- Yun, T. S., Santamarina, J. C., & Ruppel, C. (2007). Mechanical properties of sand, silt, and clay containing tetrahydrofuran hydrate. *Journal of Geophysical Research*, *112*, B04106. <https://doi.org/10.1029/2006JB004484>